



Single-phase grid interface for home energy storage

Zlatko Bosnjic · Klaus Krischan

Received: 10 October 2022 / Accepted: 13 December 2022 / Published online: 16 January 2023
 © The Author(s) 2023

Abstract In this paper, an overview of a novel home energy storage system is presented. The aim of the system is the utilization of community solar panels in urban environments with decentralized energy storage at the household level. An increase in the total energy production from renewable energy sources as well as a reduction in energy costs for the consumer are the obvious benefits of such a system. The key focus of the paper presented is to model, design, and optimize a Dual Active Bridge that serves as a low-voltage grid-battery interface for the proposed storage system. A state-of-the-art loss model of the Dual Active Bridge is presented along with a novel optimization method intended for total power loss minimization.

Keywords Power electronics · Home energy storage · Power electronic converter optimization

Einphasige Netzchnittstelle für Heimenergiespeicher

Zusammenfassung In diesem Beitrag wird ein Überblick über ein neuartiges Energiespeichersystem für Haushalte gegeben. Das Ziel des Systems ist die Nutzung von Gemeinschaftssolarpanelen in städtischen Umgebungen mit dezentraler Energiespeicherung auf der Haushaltsebene. Eine Erhöhung der Gesamtenergieproduktion aus erneuerbaren Energiequellen sowie eine Reduzierung der Energiekosten für den Verbraucher sind die offensichtlichen Vorteile eines solchen Systems.

The authors contributed equally to this work.

Z. Bosnjic (✉) · K. Krischan
 Electric Drives and Machines Institute, Graz University of
 Technology, Inffeldgasse 18/I, 8010 Graz, Austria
zlatko.bosnjic@tugraz.at

Das Hauptaugenmerk der vorliegenden Arbeit liegt auf der Modellierung, dem Design und der Optimierung einer „Dual Active Bridge“, die als Niederspannungsnetz-Batterie-Schnittstelle für das vorgeschlagene Speichersystem dient. Es wird ein neuartiges Verlustmodell der „Dual Active Bridge“ zusammen mit einer neuartigen Optimierungsmethode zur Minimierung der Verlustleistung vorgestellt.

Schlüsselwörter Leistungselektronik · Heimenergiespeicher · Optimierung leistungselektronischer Umrichter

1 Introduction

Due to ambitious targets of the European Union regarding the future of its energy supply, the need for more integration of renewable sources is rising constantly [8]. One possible area where renewable energy sources could be utilized is urban environments such as larger cities. For example, integration of a community photo-voltaic system with energy storage at the household level is a viable option. This paper outlines the structure of such a system with a focus on the bidirectional AC to DC power converter needed for grid to battery connection.

In order to find an optimal design for the power conversion stage of the proposed energy storage system, the converter topology should be firstly selected. In [3], a general overview of bidirectional DC to DC converters is outlined. For the selected application, a Dual Active Bridge with an Unfolding Bridge at the grid side is determined to be the most viable choice.

The operation of the proposed converter topology is presented in [2], along with design and optimization of the Dual Active Bridge based on minimization of the square of the Dual Active Bridge RMS currents. Minimization of the square of the RMS currents is

currently the state-of-the-art approach for Dual Active Bridge optimization. The paper at hand extends the optimization model of the Dual Active Bridge to a more general model which includes all relevant power losses. These losses include semiconductor switching losses, transformer core losses as well as gate driving losses. In comparison with the mentioned standard optimization method, the proposed method extends the operating range of the Dual Active Bridge to regions where Zero-Voltage-Switching might not be fully achieved, which is especially beneficial for lower power operation.

This paper is organized as follows: in Sect. 2 the structure of the energy storage system is outlined. The proposed design process of a line-battery interface is given in Sect. 3 along with a derivation of the mathematical model of the power converter along with a power loss model of the converter. Sect. 4 presents a novel optimization approach of the power converter. Finally, the summary of the results, as well as an outlook on further research is provided in Sect. 5.

2 Storage System Overview

As already stated in the introduction, the aim of the proposed system is decentralized energy storage, with a focus on urban environments such as larger cities. In such locations, the end user might not have the availability of a home PV system due to size and/or location. A community PV system in the vicinity of the household could still be beneficial if an energy storage system is available at the household level. The system is also able to utilize small scale photo-voltaic generation directly from the household.

The proposed energy storage system should be implemented in the form of a battery. In normal operation, the battery should serve as an energy buffer, charging when there is surplus power available, for example, during periods of the day when solar production is high. At times when the energy production is lower, the energy should be supplied back into the household and into the low-voltage grid (e.g. during peak load intervals). Additionally, the storage system should be able to operate in autonomous mode when no grid voltage is present, i.e. during a power outage. During this mode of operation, the storage system serves as a power source for a microgrid at the household level. The mentioned modes of operation are referred to as “on-grid” mode and “island” mode of operation, respectively.

A simple “Plug-and-Play” connection to the low-voltage grid is a requirement for ease of installation and ease of use. This grid connection should be achieved via a single-phase power outlet in the home. An overview of the proposed system is depicted in Fig. 1.

Total energy storage, as well as maximum power of the system are limited by the available size as well as a practical weight limits. Additionally, European stan-

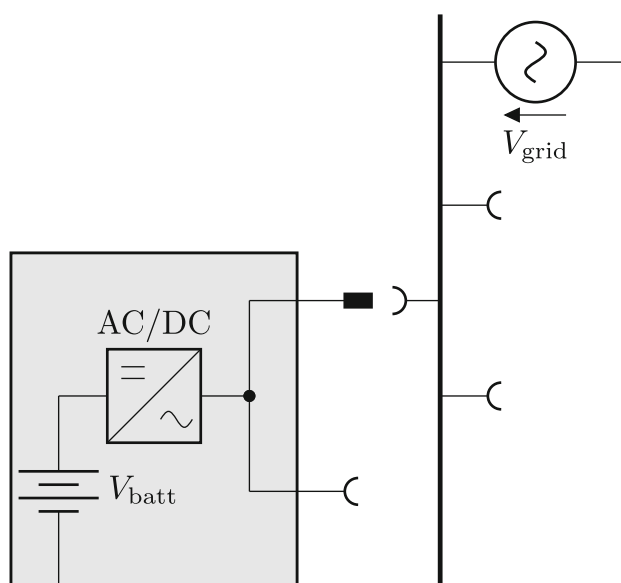


Fig. 1 LiBIF block schematic

dards and regulations for the low-voltage grid serve as an upper limit for maximal power that can be supplied into the grid. The expected energy storage capacity and power ratings (both in “on-grid” mode and “island” mode of operation) are:

- Energy storage: $E_{\text{Storage}} = 1 \dots 2 \text{ kWh}$
- On-grid power: $P_{\text{Grid}} = 800 \text{ W}$
- Off-grid power: $P_{\text{Island}} = 1000 \text{ W}$

The estimated household power consumption as well as the algorithm for minimizing total energy cost are dealt with in other publications.

3 LiBIF Structure

The central part of the proposed energy storage system is the interface between the low-voltage grid and the battery (line-battery interface, abbreviated as LiBIF). This work focuses mostly on the design, modeling and optimization of this power electronic interface.

It can be noted that AC to DC power conversion is needed when the discussed energy storage system is being charged, and DC to AC power conversion is needed when the battery is being discharged into the low-voltage grid. Therefore, the first requirement of the line-battery interface is bidirectional power flow. As is usually the case in power converter design, the following requirements should also be met:

- Small size
- Low weight
- Low cost
- High efficiency

Additionally, the adequate standards and regulations regarding power quality need be met in on-grid mode of operation.

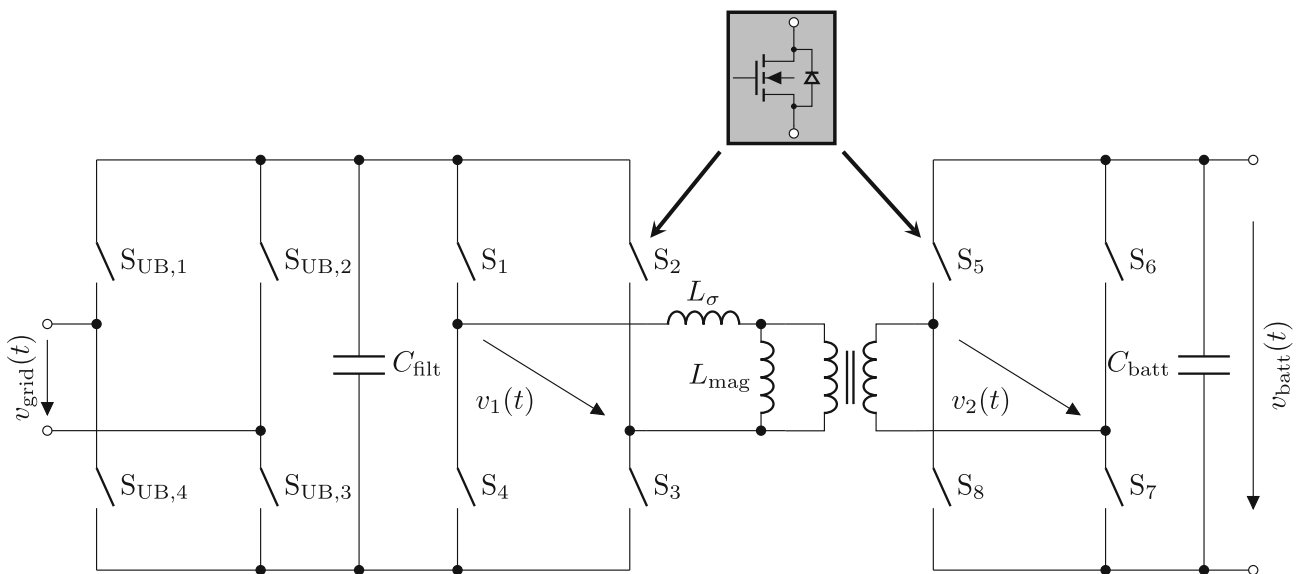


Fig. 2 Dual Active Bridge circuit schematic

Based on the given constraints a suitable converter topology was selected. Afterwards, the chosen topology was modeled and optimized.

Although the standards do not require electrical isolation, implementing the isolation of the DC-DC converter stage proved to be a more feasible solution compared to providing full isolation of the converter housing.

3.1 Topology Selection

In [6], an overview of suitable converter topologies for the given application is presented. A more detailed overview of bidirectional DC-DC converter topologies is found in [3].

Keeping the listed requirements in mind, two functions and the according building blocks of such a converter can be identified:

- Bidirectional rectification and sinusoidal line-side currents
- Isolated DC-DC conversion

One of the well known approaches for unidirectional power supplies would comprise a rectifier together with a Power Factor Correction stage and a resonant DC-DC-converter based on an LLC topology which both can be designed to allow for bidirectional power flow. The PFC stage usually includes a bulky capacitor, needed for filtering the pulsating line side power flow and to enable constant power flow to the load.

In the application at hand, however, the load (the battery) is able to handle pulsating power flow as well, thus the intermittent energy storage by the bulky filter capacitor may be omitted, and sinusoidal line side current consumption can be established by proper control of the power flow in DC-DC converter.

Controlling the transferred power flow, pulsating with twice the line voltage frequency, in presence of line side voltages ranging from zero to the peak line voltage on one side and nearly constant voltage on the other side of the isolating DC-DC converter is quite challenging to establish with an LLC based resonant circuit.

Thus, an alternative approach is followed for the application at hand, the LiBIF, comprising a line side filter, an unfolding bridge for the AC-DC interface and an (isolating) Dual Active Bridge for the DC-DC conversion and the control of the desired power flow. The chosen topology is depicted in Fig. 2.

With proper modulation, the Dual Active Bridge can be operated with virtually zero switching loss across wide input voltage ranges by employing Zero-Voltage-Switching (ZVS) [7].

A disadvantage is the need for quick and robust control due to the fact that stray inductance of the high-frequency transformer L_σ is the only current limiting element of the converter. Without proper modulation, the transformer currents can reach very high values within a single switching period which can lead to the destruction of the switches of the Dual Active Bridge. Also, the transformer core can easily saturate which leads to even higher currents in the transformer as well as in the semiconductor switches.

3.2 Modeling

An accurate mathematical model of the converter is needed for control implementation, loss approximation and finally optimization of the converter design.

Following assumptions are made for a simplified derivation of the idealized current model of the Dual Active Bridge:

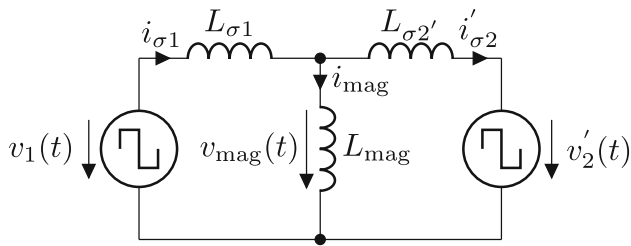


Fig. 3 Dual Active Bridge simplified circuit schematic

- The Dual Active Bridge input voltage $v_{in}(t)$ is constant over one switching period

$$v_{in}(t) \approx V_{in} \quad (1)$$

- The battery voltage $v_{batt}(t)$ is constant over one switching period

$$v_{batt}(t) \approx V_{batt} \quad (2)$$

- The total transformer leakage inductance is the sum of the leakage inductance of the primary winding (grid-side winding) and the transferred leakage inductance of the secondary winding (battery-side winding) and they are approximately equal in magnitude

$$L_{\sigma} = L_{\sigma 1} + L'_{\sigma 2} \approx 2 \cdot L_{\sigma 1} \quad (3)$$

- The total transformer leakage inductance L_{σ} is much lower than the transformer magnetizing inductance L_{mag}

$$L_{\sigma} \ll L_{mag} \quad (4)$$

Assuming the output voltages of both full-bridges of the Dual Active Bridge are pulse-width modulated square-wave voltages the simplified circuit schematic in Fig. 3 is valid for further analysis. This equivalent circuit can serve as a starting point for the derivation of Dual Active Bridge currents.

Firstly, the currents $i_{\sigma 1}$, $i'_{\sigma 2}$ and i_{mag} of the high-frequency transformer are obtained. This is summarized in the following steps. Considering the assumption that the magnetizing inductance L_{mag} is much greater than the total leakage inductance $L_{\sigma} = L_{\sigma 1} + L'_{\sigma 2}$, the voltage across the magnetizing inductance is given in Eq. (5).

$$v_{mag}(t) \approx \frac{v_1(t) + v'_2(t)}{2} \quad (5)$$

The magnetizing current $i_{mag} = i_{mag}(t)$ can be easily obtained as a solution of the differential equation (6).

$$L_{mag} \cdot \frac{d i_{mag}(t)}{d t} = v_{mag}(t) \quad (6)$$

Solving the differential equation (7), and superposing the magnetizing current $i_{mag}(t)$ with the solution, all currents of the high-frequency transformer can be obtained (Eqs. 8 and 9).

$$L_{\sigma} \cdot \frac{d i_{\sigma}(t)}{d t} = v_1(t) - v'_2(t) \quad (7)$$

$$i_{\sigma 1} = i_{\sigma 1}(t) = i_{\sigma}(t) + \frac{i_{mag}(t)}{2} \quad (8)$$

$$i'_{\sigma 2} = i'_{\sigma 2}(t) = i_{\sigma}(t) - \frac{i_{mag}(t)}{2} \quad (9)$$

Voltage waveforms $v_1(t)$ and $v_2(t)$ can be adjusted with a change in the modulation parameters of the Dual Active Bridge. Different approaches for Dual Active Bridge modulation can be found in literature [7]. Briefly, the Dual Active Bridge modulation strategies are subdivided as follows:

1. Single Phase Shift modulation (SPS) – Phase-shift angle ϕ between the full-bridge voltages is modulated
2. Dual Phase Shift modulation (DPS) – Phase-shift angle ϕ and both duty-cycles d_1 and d_2 are modulated simultaneously ($d_1 = d_2 = d$)
3. Triple Phase Shift modulation (TPS) – Phase-shift angle ϕ and both duty-cycles d_1 and d_2 are modulated independently
4. Frequency Modulation (FM) – Switching frequency f_{sw} is modulated

A general overview of modulation strategies is presented in [4]. In this paper, the most general modulation strategy will be discussed – Triple Phase Shift Modulation + Frequency Modulation. This modulation strategy offers four degrees of freedom:

1. Phase-shift angle ϕ – Angle between the positive falling edges of $v_1(t)$ and $v_2(t)$
2. Primary side duty-cycle d_1
3. Secondary side duty-cycle d_2
4. Switching frequency f_{sw}

The voltages $v_1(t)$ and $v_2(t)$ are dependent on the modulation parameters of the Dual Active Bridge. These voltages can be defined as piece-wise constant functions over half of a switching period.

$$v_1(t) = \begin{cases} V_{in}, & t \in [0, d_1) \cdot T_{sw} \\ 0, & t \in [d_1, 1/2) \cdot T_{sw} \end{cases} \quad (10)$$

$$v_2(t) = \begin{cases} V_{batt}, & t \in [d_1 + \phi - d_2, d_1 + \phi) \cdot T_{sw} \\ 0, & t \in [d_1 + \phi, 1/2 + d_1 + \phi) \cdot T_{sw} \end{cases} \quad (11)$$

As the voltages are half-wave symmetric, the definition of the voltages for the second half of the switching period is given in Eqs. 12 and 13.

$$v_1(t) = -v_1\left(t - \frac{T_{sw}}{2}\right) \quad (12)$$

$$v_2(t) = -v_2\left(t - \frac{T_{sw}}{2}\right) \quad (13)$$

Solving the differential equations 6 and 7 with voltages defined in Eqs. 12 and 13, the ideal current model as a function of circuit parameters $\{L_\sigma, L_{mag}\}$, as well as modulation parameters $\{T_{sw}, \phi, d_1, d_2\}$ is obtained.

Finally, with the obtained voltage and current mathematical expressions, a power loss model can be formulated. For the Dual Active Bridge, the total power losses P_{loss} are divided as follows:

- Conduction power losses P_{cond}
- Switching power losses P_{sw}
- Transformer core power losses P_{core}
- Gate driving losses P_{dr}

Conduction power losses are defined as losses that occur in the power semiconductor switches and in the high-frequency transformer windings:

$$P_{cond} = i_{\sigma 1, RMS}^2 \cdot R_1 + i_{\sigma 2, RMS}^2 \cdot R_2 \quad (14)$$

where R_1 is the sum of the resistances of the primary-side power semiconductor switches and the transformer primary winding resistance.

$$R_1 = 2 \cdot R_{ds(on),1} + R_{wdg1} \quad (15)$$

Equivalently, R_2 is the sum of the resistances on the transformer secondary side.

$$R_2 = 2 \cdot R_{ds(on),2} + R_{wdg2} \quad (16)$$

The switching power loss model includes the hard-switching loss range of operation, partial hard-switching range of operation as well as the soft-switching range of operation. During hard-switching, the losses per semiconductor switch are derived from the data-sheet parameters as well as the imposed voltages and currents on the semiconductor switch. For partial hard-switching, the losses are calculated based on the stored charge that remains in the switch capacitances after a resonant transition. For soft-switching (sometimes referred to as Zero-Voltage-Switching), only the body diode conduction losses are taken into account. The analytical derivation of the loss model is described in [1].

Transformer core power losses P_{core} are derived from the improved Generalized Steinmetz Equation (iGSE). The empirical method is discussed in [5].

Gate driving losses P_{dr} are a function of the MOSFET driving voltage V_{dr} , the switching period T_{sw} as well as MOSFET gate charge Q_g .

$$P_{dr} = \frac{4}{T_{sw}} \cdot (Q_{g1} \cdot V_{dr1} + Q_{g2} \cdot V_{dr2}) \quad (17)$$

The total losses P_{loss} are defined as a sum of the listed losses for one set of modulation parameters over one switching period.

$$P_{loss} = P_{cond} + P_{sw} + P_{core} + P_{dr} \quad (18)$$

4 Dual Active Bridge Optimization

As described in Sect. 3, the most general modulation case of the Dual Active Bridge is Triple Phase Shift Modulation with Frequency Modulation. This modulation strategy guarantees lowest overall losses for a given set of Dual Active Bridge circuit parameters. A vector of the four modulation parameters is defined in Eq. 19. These parameters are independent variables that offer four degrees of freedom for the optimization.

$$\mathbf{x} = \begin{bmatrix} T_{sw} \\ \phi \\ d_1 \\ d_2 \end{bmatrix} \quad (19)$$

With a fixed set of Dual Active Bridge circuit parameters $\{L_\sigma, L_{mag}, N, R_1, R_2\}$ and with known semiconductor switches, the search for a vector of modulation parameters \mathbf{x} that minimize a given cost function defines the optimization problem outlined in this section. For the given application, a grid-battery interface, overall Dual Active Bridge losses P_{loss} were selected as the cost function for optimization. The mathematical formulation of the optimization problem is given in Eq. 20.

$$\mathbf{x}_{opt} = \underset{\mathbf{x} \in \Omega}{\operatorname{argmin}} P_{loss}(\mathbf{x}) \quad (20)$$

s.t. $I_{in}(\mathbf{x}) = I_{in, set}$

Ω is a 4D, bounded search space of the modulation parameters:

$$\Omega := \left\{ T_{sw} \in (T_{sw, min}, T_{sw, max}), \phi \in \left[\frac{-1}{4}, \frac{1}{4} \right], \right. \\ \left. d_1 \in \left(0, \frac{1}{2} \right], d_2 \in \left(0, \frac{1}{2} \right] \right\} \quad (21)$$

$I_{in}(\mathbf{x})$ is a non-linear constraint of the optimization problem which defines the switching period averaged input current drawn from the grid-side of the Dual Active Bridge.

As the voltage imposed on the grid-side of the Dual Active Bridge $v_{in}(t)$ is not constant, the optimization procedure needs to be repeated for different values of the input voltage. Additionally, the set-point of the input Dual Active Bridge current should be varied to

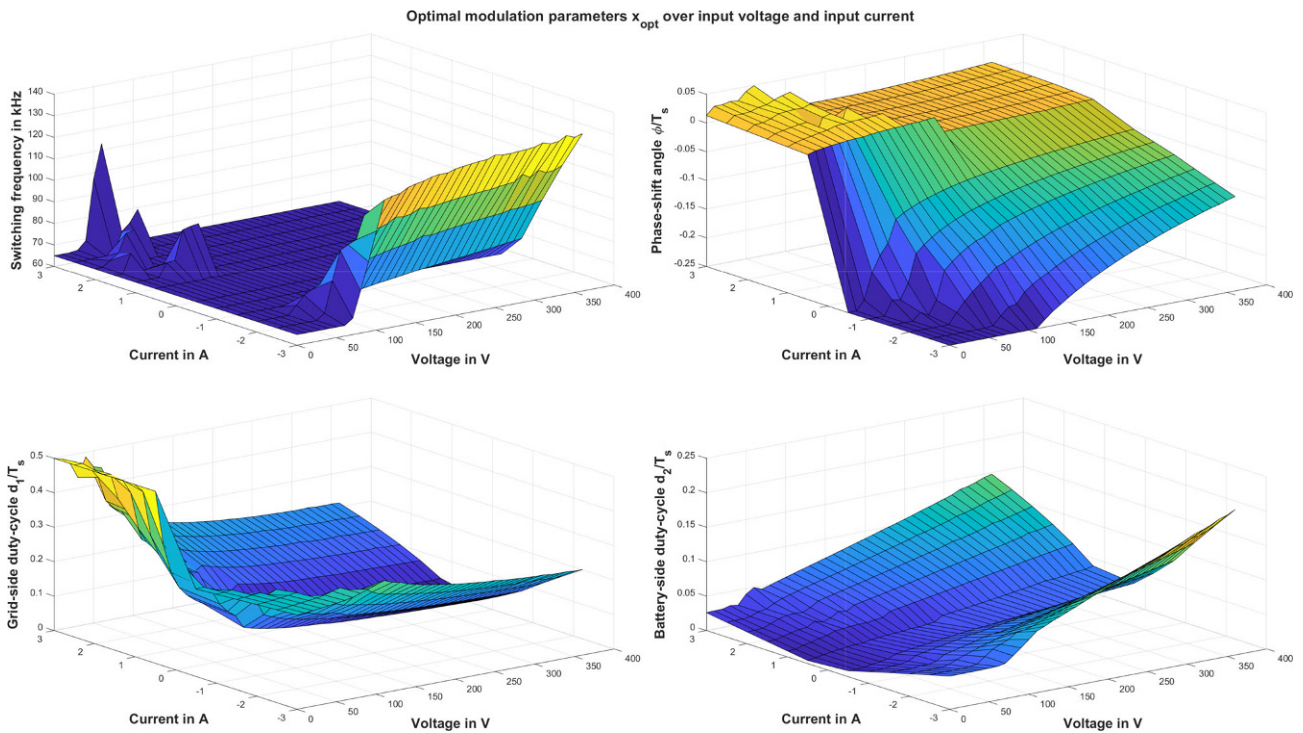


Fig. 4 Optimal modulation parameters x_{opt}

ensure sinusoidal grid current $I_{in,set}$ when the input voltage is varied.

$$v_{in}(t) = \widehat{V}_{grid} \cdot |\sin \omega_L \cdot t| \quad (22)$$

$$i_{in}(t) = \widehat{I}_{grid} \cdot |\sin \omega_L \cdot t| \quad (23)$$

As an example, in Fig. 4, the sets of optimal modulation parameters x_{opt} are depicted. The optimization was performed with circuit parameters shown in Table 1 for an input voltage range $V_{in} \in [0,350]$ V and an input current range $I_{in} \in [-3.5,3.5]$ A.

From the subplots in Fig. 4 it can be observed that all the modulation parameters vary smoothly with variation of the input voltage V_{in} and with variation of the input current I_{in} . This behavior is beneficial as it enables stable operation of the Dual Active Bridge

Table 1 Circuit parameters used for optimization

Parameter	Value	Unit
L_σ	30	μH
L_{mag}	200	μH
N	10	–

Table 2 Modulation parameters bounds used for optimization

Parameter	Lower bound	Upper bound	Unit
T_{sw}	4.00	15.38	μs
ϕ	-0.25	0.25	–
d_1	0.00	0.50	–
d_2	0.00	0.50	–

without steps in any of the modulation parameters during expected operation.

As can be seen in the first subplot, the switching frequency $f_{sw} (= 1/T_{sw})$ is constant and equal to the lower set bound (shown in Table 2) for most of the operating range. The lower bound for the switching frequency is a limit of the pulse pattern generation of the test hardware. An increase in the switching frequency is observed in the range of high negative currents. The switches of the Dual Active Bridge operate with partial hard switching in this range and therefore the switching frequency can be increased to lower RMS currents and conduction losses at the expense of slightly higher switching losses. Deviation from the lower bound of the switching frequency is also observed for some operating points with low input voltage and positive input current which can be attributed to imprecision of the optimization algorithm or to the change in the operating range of the Dual Active Bridge.

In the second subplot of Fig. 4, the phase-shift angle ϕ of the Dual Active Bridge is depicted. As is expected, for negative input currents the phase-shift angle is negative and positive for positive input currents. A discontinuity in the phase-shift angle can be observed for positive input current and low input voltage which can be explained by a change from ZVS to non-ZVS mode of operation of the Dual Active Bridge.

The third and fourth subplot in Fig. 4 show the behavior of the grid-side and battery-side duty-cycles of the Dual Active Bridge, respectively. From the plots, it can be observed that there is an increase in both duty-cycles as the absolute value of the input current

is increased. Similarly to both the switching frequency and phase-shift angle, there is some discontinuity in the duty-cycles for positive input currents and low input voltages.

5 Conclusion and Outlook

An overview of a development process of a bidirectional low-voltage AC/DC converter for home energy storage has been presented. The AC/DC converter topology was selected, modeled and optimized with lowest overall losses in mind. The loss model of the Dual Active Bridge converter has been extended to include total converter losses. Also, the optimization procedure was performed with the most general modulation Dual Active Bridge modulation strategy (TPS + FM). The results have been presented in Fig. 4.

Further work on this topic might include a comparison of the proposed loss model and optimization method with the optimization methods relying only on conduction loss minimization (e.g. in [2]). Additionally, the optimization method could be extended to include size, weight and cost minimization. Validation of the loss model with experimental results is of interest as well.

Acknowledgements This work was supported in part by the Austrian Research Promotion Agency (FFG) and in cooperation with EET – Efficient Energy Technology GmbH. Funding for this project was provided by the Austrian Research Promotion Agency (FFG).

Funding Open access funding provided by Graz University of Technology.

Open Access This article is licensed under a Creative Commons Attribution 4.0 International License, which permits use, sharing, adaptation, distribution and reproduction in any medium or format, as long as you give appropriate credit to the original author(s) and the source, provide a link to the Creative Commons licence, and indicate if changes were made. The images or other third party material in this article are included in the article's Creative Commons licence, unless indicated otherwise in a credit line to the material. If material is not included in the article's Creative Commons licence and your intended use is not permitted by statutory regulation or exceeds the permitted use, you will need to obtain permission directly from the copyright holder. To view a copy of this licence, visit <http://creativecommons.org/licenses/by/4.0/>.

References

- Christen D, Biela J (2019) Analytical switching loss modeling based on datasheet parameters for mosfets in a half-bridge. *IEEE Trans Power Electron* 34(4):3700–3710. <https://doi.org/10.1109/tpel.2018.2851068>
- Everts J (2014) Modeling and optimization of bidirectional dual active bridge ac–dc converter topologies. Phd thesis, KU Leuven
- Gorji SA, Sahebi HG, Ektesabi M, Rad AB (2019) Topologies and control schemes of bidirectional DC–DC power converters: An overview. *IEEE Access* 7:117,997–118,019. <https://doi.org/10.1109/access.2019.2937239>
- Hou N, Li YW (2020) Overview and comparison of modulation and control strategies for a nonresonant single-phase dual-active-bridge DC–DC converter. *IEEE Trans Power Electron* 35(3):3148–3172. <https://doi.org/10.1109/tpel.2019.2927930>
- Li J, Abdallah T, Sullivan C (2001) Improved calculation of core loss with nonsinusoidal waveforms. In: Conference Record of the 2001 IEEE Industry Applications Conference. 36th IAS Annual Meeting (Cat. No.01CH37248) <https://doi.org/10.1109/ias.2001.955931>
- Salcher P (2021) Bidirektionale Ladeschaltung. Master's thesis, Graz University of Technology
- Shah SS, Iyer VM, Bhattacharya S (2019) Exact solution of ZVS boundaries and AC-port currents in dual active bridge type DC–DC converters. *IEEE Trans Power Electron* 34(6):5043–5047. <https://doi.org/10.1109/tpel.2018.2884294>
- Wolf S, Teitge J, Mielke J, Schütze F, Jaeger C (2021) The european green deal — more than climate neutrality. *Interconomics* 56(2):99–107. <https://doi.org/10.1007/s10272-021-0963-z>

Publisher's Note Springer Nature remains neutral with regard to jurisdictional claims in published maps and institutional affiliations.



Zlatko Bosnjic, received the B.o.E. (B.Sc.) degree in electrical engineering from the University of Sarajevo, the Dipl.-Ing. degree in electrical engineering from Graz University of Technology in 2017 and 2021 respectively. He is currently working as a research assistant at the Electric Drives and Machines Institute, Graz University of Technology.



Klaus Krischan, born in 1965, studied electrical engineering at Graz University of Technology. After finishing his PhD he joined the Electric Drives and Machines Institute at Graz University of Technology as a research assistant. His research interests are in the field of power electronics, especially in the area of drive technology.